Journal of ENVIRONMENTAL Treatment Techniques

J. Environ. Treat. Tech.
ISSN: 2309-1185

Journal web link: http://www.jett.dormaj.com
https://doi.org/10.47277/8(3)1241

Enhanced Degradation of Reactive Black 5 from Aqueous Solution over TiO_2 Nanoparticles under UV Light Irradiation: Optimization, Experimental & Theoretical Approaches

Sabah Shiri[1], Mohsen Mehdipour Rabori[2], Zeinab Gholami[3], Zeinab Rahmati[4], Moayed Adiban[5]*, Mansour Sarafraz[3]*

[1]Department of Chemistry. Payame Noor University. P.O. Box 19395-4697, Tehran, Iran
[2]Environmental Health Engineering Research Center, Kerman University of Medical Sciences, Kerman, Iran and Department of Environmental Health, School of Public Health, Kerman University of Medical Sciences, Kerman, Iran
[3]Student Research Committee, School of Public Health, Tehran University of Medical Sciences, Tehran, Iran
[4]Department of Environmental Health Engineering, School of Public Health, Ilam University of Medical Science, Ilam, Iran
[5]Department of Environmental Health Engineering, School of Public Health, Ilam University of Medical Science, Ilam, Iran.
[6]Student Research Committee, School of Public Health and Safety, Shahid Beheshti University of Medical Sciences, Tehran, Iran

Received: 06/01/2020 Accepted: 13/04/2020 Published: 20/09/2020

Abstract

In this study, the elimination of dye from contaminated water was considered by the photocatalytic process with TiO_2. The effects of operational parameters like TiO_2 dosage, initial dye concentration, pH, contact time and temperature on the rate of dye decomposition are studied. TiO2 nanoparticles were characterized by XRD, FESEM, and FTIR. The Response Surface Methodology was carried out to investigate the composition effect of input independent factors and removal efficiency (one dependent output response). The F-value (315.9), P-value ($2.2 \times 10{-}16$), multiple R^2 (0.9858), adjusted R^2 (0.9827), and lack of fit (0.494) show that the reduced second-order model is greatly significant for dye removal by TiO_2 nanoparticles. The efficacy of the process at the optimum operating conditions, pH=11, TiO_2 dose (0.7 g/l), reaction time (67.5 minutes), Temperature (40 °C), and initial dye concentration (55 mg/l) was 86.6%. By using regression coefficients derived from the model and the Solver "Add-ins", higher removal efficiency was accounted to be 90%. The results showed that the TiO_2 nanoparticles under UV light irradiation are very proper for reducing the concentration of pollutants in textile wastewater effluent.

Keywords: TiO_2, Photocatalytic degradation, Reactive black 5**,** Optimization, UV light

1 Introduction

Annually about 70 tons of colors are produced worldwide (1). Dyes, have a complex molecular structure and are often toxic, carcinogenic (production of amine groups in the anaerobic decomposition), mutagenic, non-biodegradable and consistent (2, 3). The use of dye in the textile, leather, paper, ceramics, cosmetics, ink and plastic industries and the entry effluents of these industries in water resources, is a major environmental problem (4, 5). Dye sewage and other effluents from these industries create several problems in terms of operation in the wastewater purification (6). Removal of dye from wastewater is often more important than the removal of other organic compounds because the presence of small amounts of dyes (below 1 ppm) is obviously visible and leaves a significant impact on the water bodies (7, 8). Discharge of colored wastewaters to the environment are leading eutrophication, interference in the ecology, affecting the intensity of photosynthesis of aquatic plants and algae (9). For dye removal from wastewater can be used as physical, chemical and biological methods (10). Because of the color stability against biodegradation, often for the removal of dyes have been used physical and chemical methods such as coagulation, flocculation, adsorption, chemical oxidation, and membrane processes. Often decomposition of materials via conventional treatment processes mayhap difficult. Therefore, it is essential to use more efficient treatment processes for demolition of these contaminants (11-14). Among the various wastewater treatment technologies, some systems such as advanced oxidation processes (AOPs) due to the production of very passive and oxidizing free radicals, have gained much attention. (15-17). In general, among AOPs the semiconductor photocatalysis is one of the most efficient destructive technologies for the complete elimination and full mineralization of undesirable organic pollutants (18-22). Titanium dioxide (TiO_2) as a semiconductor photocatalyst due to high oxidation power, photochemical stability, large surface area to volume ratio, low toxicity and low cost, are widely used as catalysts in photocatalysts reactions (23-27). To survey the

***Correponding author:** (a) Moayed Adiban, Department of Environmental Health Engineering, School of Public Health, Ilam University of Medical Science, Ilam, Iran. E-mail: adiban-m @medilam.ac.ir. (b) Mansour Sarafraz, Student Research Committee, School of Public Health and Safety, Shahid Beheshti University of Medical Sciences, Tehran, Iran. E-mail: mansour.sarafraz@yahoo.com

effects of various parameters, the interactions of the experimental variables and reduce number of required experiments was used the statistical RSM technique (28). The RSM is a statistical method that was used for experimental design to assig the amounts of process factors, experiential modeling to estimate the relationship among factors and responses and optimization of the operating conditions in the independent variables (29). The morphology and structure of the nanocrystalline TiO_2 were determined by XRD, FESEM and FTIR. The effect of some parameters such as temperature, catalyst dosage, the concentration of the dye and time were investigated. The aims of this study were characterized by TiO_2 nanoparticles, investigation of photo-degradation efficiency of Reactive Black 5 dyes, and optimization of main operational factors such as TiO2 dosage, solution pH, dye concentration, time and temperature by RSM. The innovations of this study were to investigate the effect of the Tio2 / UV process for the first time on the destruction of dyes with more complex structures such as Reactive black 5.

2 Materials and methods

2.1 Materials

De-ionized water is used to prepare all of the chemicals and standard solutions. Nanoparticles of P-25 TiO_2 (mainly in anatase form), with an average particle size less than 30 nm, the specific surface area (BET) of 50±15 m^2/g and purity greater than 99.5% from Degussa (Germany) was used as the photo-catalyst without further treatment. The reactive Black-5 dye with the chemical structure $C_{26}H_{21}Na_4N_5O_{19}S_6$ and a molecular weight of 1029.88 g/mol as the sorbate in this study was provided from Alvan Sabet in Iran. To immobilization of TiO_2 on Borosilicate glass plates (150mm × 150mm), commercially available Titanium powder such as peroxide P25 mixed with a solvent. Then coating was done by pipetting methods. In pipetting the substrate was left to dry until most of the solvent evaporated. After sintering at high temperature (400-600 °C) the film will adhere to the substrate (30). The distance between the UV lamps and TiO_2 films were 1.5 cm.

2.2 Photocatalytic experiments

The reactor used for photocatalytic oxidation of RB-5 dye by UV/TiO_2 is shown in Figure 1. This reactor consists of two outer and inner parts, which A UV-lamp with 128 W medium-pressure, 220 V and maximum wavelength at 247.3 nm as the radiation source is placed in the inner part. The outer portion of the reactor should be contained 2 L solution for keeping the solution at $25 \pm 2\ ^{\circ}C$. All irradiation experiments of dye solution were performed by stirring 1000 ml of dye solution with immobilized TiO_2 and during the experiment, the solution in the reactor was constantly stirred. After preparing the Stock solution (1000 mg/L) of RB-5, photo-degradation dye experiments of dye were conducted in a batch reactor by using evaluation of the effect of pH (2 to 11), initial dye concentrations (10 to 100 mg L^{-1}), contact time (15 to 120 minutes), TiO_2 dose (0.2 to 1.2 g L^{-1}) and temperature (20 to 60 $^{\circ}C$). According to five variables pH, dye concentration, contact time, TiO_2 dose and temperature, to do the tests were determined 62 runs by using the software R. Dye concentration for the samples were performed by spectrophotometer (DR5000, HACH LANGE, USA) according to standard method at a wavelength of 598 nm (31). For each experiment, the dye removal percentage (R%) was calculated using *Eq.* (1):

$$R = \frac{C_0 - C_t}{C_0} \times 100 \quad (1)$$

where C_0 is the initial dye concentration and C_t, is the concentration of dye at intervals of the irradiation time. Surface morphology and characteristics of P-25 TiO_2 nanoparticles were subjected by using XRD, FESEM and FTIR technology. X-ray diffraction patterns of the samples were done by an X' Pert Pro (PerkinElmer, Netherland) diffractometer, with Cu Kα radiation (λ =1.54060 å), Generator settings = 40 kV, 40 mA and the 2θ range from 10 to 80°. The average dimension (D) of particles was calculated based on the diffraction of peak broadening using the Debye–Scherrer's *Eq 2* (32):

$$D = \frac{k\lambda}{\beta cos\theta} \quad (2)$$

where λ is the X-ray wavelength of the Cu Kα radiation (nm), β is the peak width of the diffraction peak profile at half the maximum height, which results from the small crystallite size (radians), and K is a coefficient related to a crystalline shape which is normally equal to 0.9. The morphological features and surface characteristics of TiO_2 were investigated using a Field Emission Scanning Electron Microscopy (FESEM) unit (MIRA3, TE-SCAN, Czechoslovakia). Fourier-transform infrared spectroscopy (FTIR), is another characterization technique was obtained using (Spectrum Tow PerkinElmer, USA). Statistical analysis also was carried out by using the software R.

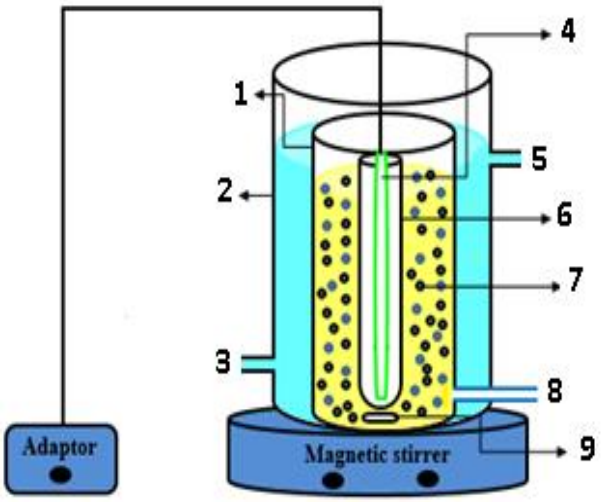

Figure 1: Schematic diagram of the experimental photoreactor: (1) reaction chamber, (2) outlet chamber, (3 cooling water inlet, (4) LED lamp, (5) cooling water outlet, (6) quartz tube, (7) nano particles, (8) sampling port, (9) magnet

2.3 Experimental Design with Response surface method (RSM)

RSM is an efficient statistical tool that was employed in the data analysis, statistical design of the experiments, and optimizing the operating conditions in independent variables (33). In RSM two designs have been used, which include: Box Behnken Design (BBD) and Central Composite Design (CCD). In this study, numbers of experiments were carried out according to a CCD for predicting and modeling the complicated relations between input-independent factors (pH(X_1), initial dye concentration(X_2), reaction time(X_3), TiO_2 dose(X_4), and temperature(X_5)) and determining the dye removal efficiency(Y) under the optimum operational conditions (34). The real values of the independent variables that were used to the experimental design are presented in Table 1.

Table 1: Coded values of independent variables used for experimental design

Variable		Coded level		
		-1	0	1
		values		
pH	x_1	2	6.5	11
TiO_2 (gr L^{-1})	x_2	0.2	50.7	1.2
Time (min)	x_3	15	67.5	120
Temp ($°C$)	x_4	20	40	60
Conc. RB_5 (mg L^{-1})	x_5	10	55	100

The Independent variables were varied over five levels as -1, 0, and 1, respectively at the determined ranges based on a set of preliminary experiments. The experimental design was conducted using R software for Windows (version 3.0.3:6 March 2014). The total number of experiments according to *Eq. (3)* were conducted for the five factors.

$$\text{No: of Experiments} = 2^k + 2k + 20 \quad (3)$$

Totally, 62 runs were designed using a 32 full factorial (the base design), 10 axial points and 20 replicates in the center point (35).
A quadratic model as *Eq. (4)* was used to express the interaction between (Y) and (X_1, X_2, X_3, X_4 and X_5):

$$\gamma = B_0 + \sum_{i=1}^{k} B_i X_I + \sum_{I=1}^{K} B_{ii} X_i^2 + \sum_{i=1}^{k-1} \sum_{j=1}^{k} B_{IJ} X_I X_J + C \quad (4)$$

where B_0 is the intercept value, B_i, B_{ii}, and B_{ij} refer to the regression coefficient for linear, second- order, and interactive effects respectively, X_i and X_j are the independent variables, and C denotes the error of prediction (36-38).

3 Results and discussion

3.1 Characterization of the TiO_2 nanoparticles

Physical, chemical and morphological properties of the TiO_2 nanoparticles were specified by means of various techniques including X-ray powder diffraction (XRD), scanning electron microscopy (FESEM) and Fourier transform infrared spectroscopy (FTIR). To evaluate the structure, nature and size of TiO_2 crystalline phases was first performed XRD analysis as presented in Fig. 2. The XRD analysis illustrates the diffraction pattern and the mineralogical composition of the TiO_2 nanoparticles. According to the Debye– Scherrer formula, the average crystallite size based on the half-width of the most intense peak (101) was estimated 30 nm, suggesting an achievement to nanoscale crystals. In investigate of Figure 1, can observe several Titania crystalline peaks for sample at 2θ = 25.4(101), 37.9(004), 48.0(200), 54.5(211), 62.6(204), 69.5(116) and 75.2(118) [JCPDS No. 71 -1167 were a = 3.786Å and c = 9.507Å] which indicates the existence of the anatase phase (39). Field emission scanning electron microscopy, affords topographical and fundamental information with virtually unlimited depth of field. The FESEM images of the TiO_2 nanoparticles before (A) and after (C) of degradation process are presented in Fig 3. As observed in Fig. 3A, nanoparticles are spherical and scattered in different sizes (20–60 nm). The surface of this TiO_2 nanoparticles shows irregular texture with finer particle size. Further, there are holes between particles that show the porous structure of this material. In some places the nanoparticles are compact in mass, but in general, optimum dispersion of particles in the surface is observed. After of the degradation process no noticeable changes were noticed in the surface morphology of the TiO_2 nanoparticles (Fig. 3C).

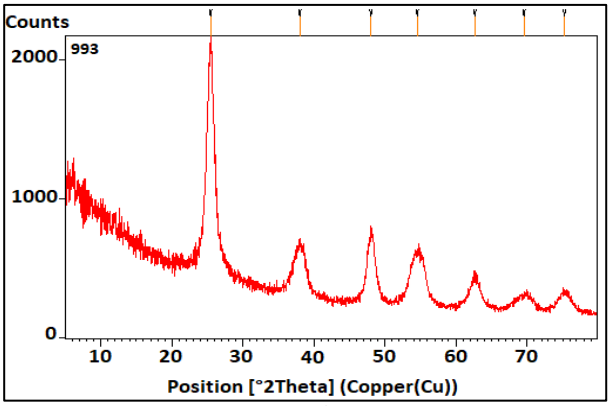

Figure 2: XRD pattern of TiO_2 nanoparticles

Energy-dispersive X-ray spectroscopy (EDS) is an analytical technique that performed for the elemental analysis of a sample. The EDS spectra of the TiO_2 nanoparticles, before (B) and after (D) of dye removal in order to survey their localized elemental information are shown in Fig 3B. Oxygen and Titania are the elements throughout the surface of the TiO_2 nanoparticles before removing the dye with weight percentages of 43.1 and 56.9 respectively. Therefore the existence of TiO_2 was confirmed. After removing the dye O, Ti, C, Na, S, and N are the elements throughout the surface of the TiO_2 nanoparticles with weight percentages of 43.6, 42.0, 14.4, 0.1, 0.0 and 0.0%, respectively. So after removing the dye with TiO_2 nanoparticles, these elements are added in Fig. 3D (40, 41). To control frequency changes in the functional group of the photocatalyst and in order to investigate the surface characteristics of the TiO_2 nanoparticles before and after degradation of reactive black 5 dye, was considered the by using Fourier transform infrared spectroscopy (FTIR) spectra in the range of 400-4000 cm^{-1} (Figures 4A and B). The FTIR spectrum of TiO_2 nanoparticles before the degradation of dye illustrates that the peak positions are at 3390, 1631, 792 cm^{-1}. The degradation band at ~3390 cm^{-1} was the characteristic peak of alcohol and phenol groups due to the symmetric stretching vibration of OH. The intense broad peak at ~1631cm^{-1} is assigned in the bending vibration of the C=O bond. Furthermore, the small peak at ~792 cm^{-1} can be allocated to the bending vibration of the N–H bond. The FTIR spectrum of TiO_2 nanoparticles after removal of dye shows the peak at 3388, 1628 and 783 cm^{-1}. The bond at 3388 specifies OH of alcohol and phenol groups, 1628 shows C–H of amide group and 783 illustrates N–H of Amine group (42-44).

3.2 Quadratic models for degradation photocatalytic of dye via the TiO_2 nanoparticles

To survey the individual and combined effects of variables on dye removal efficiency, degradation experiments were carried out at the specified combinations of the physical parameters. The CCD design matrix was done to evaluate the contribution of five influential factors including pH, TiO_2 dosage, time, temperature and dye concentration. The experimental design of 62 runs along with the experimental and the predicted data for the removal of dye by TiO_2 nanoparticles in the CCD experimental design are shown in Table 2. To identify the optimum conditions, the RSM results need to be studied along the optimization process (45).

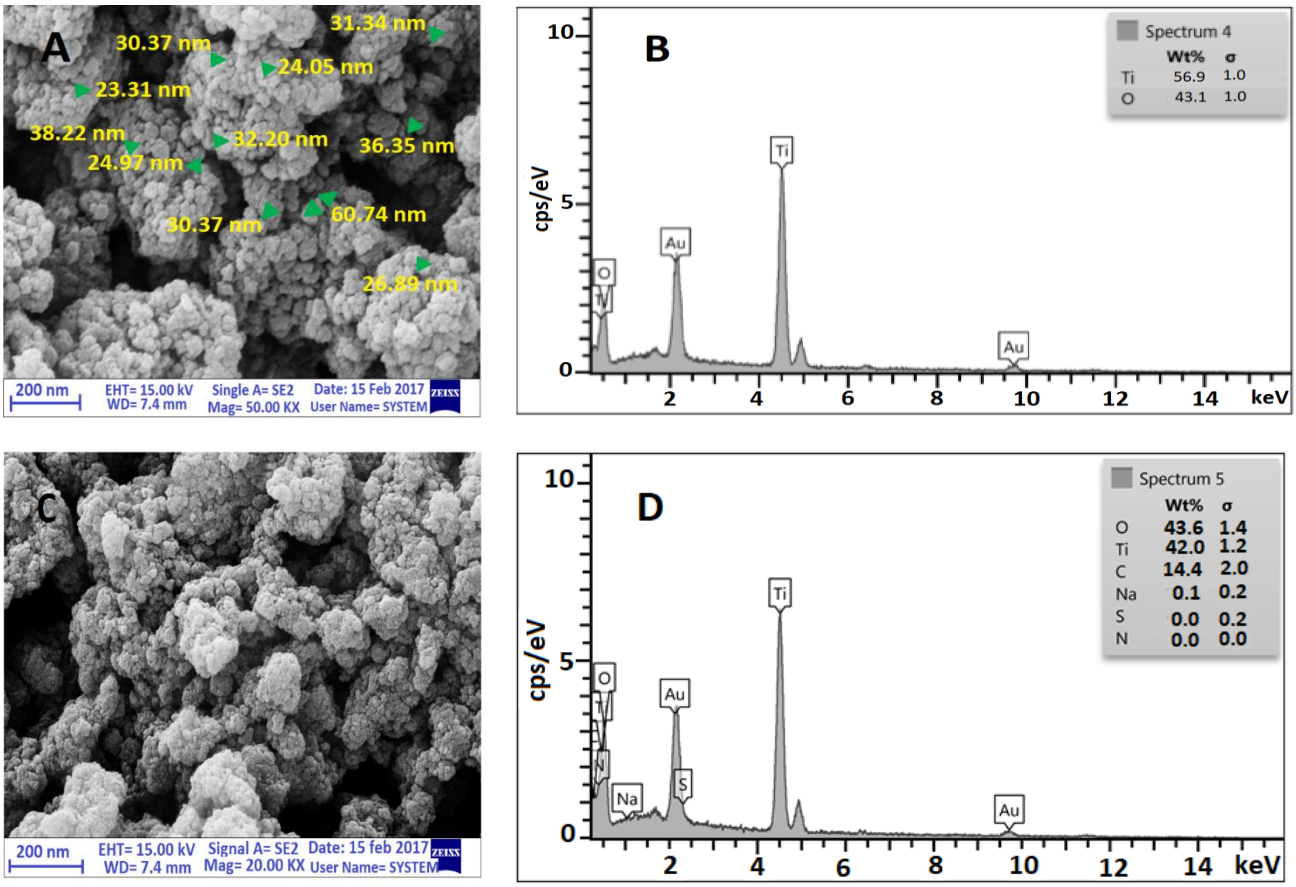

Figure 3: FE-SEM image and EDS spectrum of TiO_2 nanoparticles before (A, B), and after (C, D) of dye removal

From Table 2, it can be seen that the dye removal values are between 26.40% (Run 15) and 86.60% (Run 54). Moreover, the lowest dye removal efficiency has been understood in runs numbers 12, 15, 28, 30, 31, 38 and 39, that the main reasons for decreasing removal, can be lower pH level and/or lower TiO_2 dosage. When the TiO_2 dose and pH level are low, e.g. run 12, the synergistic effect was very significant and the dye removal efficiency reduced intensity. According to the Table 2, the time and temperature have low significant effects on dye removal with TiO_2 nanoparticles (run numbers of 12, 15 and 38). Run 54 was obvious as optimum condition, because it indicated the highest removal efficiency, and also the pH is a very fundamental parameter in water treatment plants. However, the pH, TiO_2 dosage and dye concentration were appropriate as optimum conditions. The pH in acidic range may induce serious operational difficulties in water treatment processes. So, economically the conditions for run 54 with pH 11, Initial dye concentration of 55 mg L^{-1}, Time of 67.5 min, Temperature of 40 ℃ and TiO_2 dosage of 0.7 g L^{-1} are the better runs.

3.3 Development of regression model equation and model analysis

The reduced quadratic model was generated by multiple regression analysis on the experimental data, and are shown in Table 3. According to the table 3, it is observable that the pH (X_1), TiO_2 dosage (X_2) and time (X_3) are significant (p-values < 0.05), so three terms available in Table 3 could influence the model formulation. In this table can be seen that pH (X_1), TiO_2 dosage (X_2), time (X_3), X_1:X_2, X_3:X_4 and X_3^2 have synergistic effect on the response prediction by the model, while X_2:X_5, X_2^2 and X_5^2 have antagonistic effect.

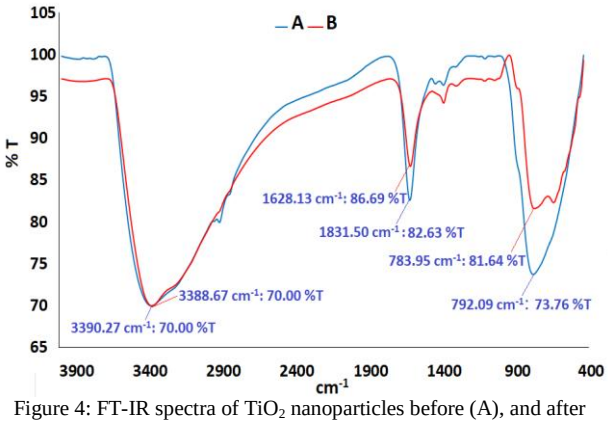

Figure 4: FT-IR spectra of TiO_2 nanoparticles before (A), and after (B) degradation of dye

Dye removal efficiency predicted by the model is shown in the Table 2. When the response predicted by the model and experimental data acquired in the laboratory have a correlate linearly, the model is dependable (46). The equations of the quadratic model, for both coded and uncoded values of the parameters, are presented at Eqs.4 and 5, respectively. Therefore, these models can be used for prediction and optimization (47-49).

$$Y_{Dye} = 10.74 + 4.343X_1 + 39.84X_2 - 0.1204X_3 + 0.2681X_5 + 0.497X_1X_2 - 0.03891X_2X_5 + 0.000714X_3X_4 - 22.27X_2^2 + 0.000812X_3^2 - 0.00228X_5^2 \quad (4)$$

$$\gamma_{Dye}=60.98065+21.10893X_1+4.87979X_2+0.93225X_3+1.11835X_1X_2-0.87540X_2X_5 +0.75011X_3X_4-5.56679X_2^2+2.23775X_3^2-4.61225X_5^2 \quad (5)$$

The model adequacy can be made clear from ANOVA analysis; R^2 and R^2adj are presented in Table 4. The ANOVA analysis is a statistical technique that in this technique, statistical significance and accuracy of the models can be predicted via high *F*, low *p*-value, correlation coefficient (*R*), and the results of lack of fit test (50). Also if *p*-value less than 0.05 shows the model terms are significant and the values greater than 0.10 indicate they are not significant. The lack of fit value parameter reflected the variation of response around the fitted model; this parameter should be insignificant if the model fits data well (51). According to the ANOVA analysis, the higher *F*-value of 315.9 with a *p*-value lower than 0.0001 as shown in Table 4 indicates that the second-order polynomial model is statistically significant, thus the model 652.17 and 65.83 respectively, that shows the model and the individual coefficients of the model are more significant. The lack of fit value of the model available in Table 4, i.e. 0.494, indicates the significant correlation between factors and dye removal as a response.

Table 2: CCD experimental design for RB5 removal by TiO_2 nanoparticles

Run	Independent factors					Expt. Removal (%)	Pred. Removal (%)	Run	Independent factors					Expt. Removal (%)	Pred. Removal (%)
	X_1	X_2	X_3	X_4	X_5				X_1	X_2	X_3	X_4	X_5		
1	2	1.2	120	60	100	37.1	38.10	32	2	1.2	120	20	100	34.7	34.67
2	11	1.2	120	20	10	83.4	81.75	33	11	0.2	120	60	100	70.6	72.32
3	6.5	0.7	67.5	40	55	61.3	62.06	34	6.5	0.7	67.5	40	55	57.8	62.06
4	2	1.2	15	20	100	32.6	34.30	35	11	0.2	15	60	100	69.3	68.95
5	6.5	0.7	67.5	40	55	60.7	62.06	36	2	1.2	15	60	100	34.8	34.73
6	11	1.2	120	20	100	78.7	79.13	37	11	0.2	120	20	100	68.5	68.89
7	6.5	0.7	67.5	40	55	60.9	62.06	38	2	0.2	15	60	100	27.8	28.97
8	6.5	0.7	67.5	40	55	58.1	62.06	39	2	0.2	15	20	10	30.3	27.66
9	11	0.2	15	20	100	66.6	68.52	40	11	0.2	120	60	10	67.2	71.44
10	11	1.2	15	20	10	80.3	81.38	41	6.5	0.7	67.5	40	55	55.6	62.06
11	6.5	0.7	67.5	40	55	62.7	62.06	42	2	1.2	15	60	10	33.7	37.36
12	2	0.2	120	60	100	27.9	32.34	43	6.5	0.7	67.5	40	55	60.6	62.06
13	11	1.2	120	60	10	84.8	85.18	44	6.5	0.7	67.5	40	55	58.9	62.06
14	11	0.2	15	60	10	68.9	68.07	45	6.5	0.7	67.5	40	55	59.2	62.06
15	2	0.2	15	60	10	26.4	28.09	46	2	0.7	67.5	40	55	35.3	40.95
16	6.5	0.7	67.5	40	55	63.3	62.06	47	6.5	0.7	67.5	40	55	61.1	62.06
17	2	1.2	120	20	10	36.2	37.30	48	6.5	1.2	67.5	40	55	59.9	61.37
18	11	1.2	15	60	10	77.4	81.81	49	6.5	0.7	67.5	40	55	60.5	62.06
19	6.5	0.7	67.5	40	55	60.3	62.06	50	6.5	0.7	67.5	40	55	62.5	62.06
20	2	1.2	120	60	10	40.6	40.73	51	6.5	0.7	15	40	55	61.7	62.67
21	11	1.2	120	60	100	79.7	82.56	52	6.5	0.7	67.5	40	10	56.8	57.88
22	11	1.2	15	60	100	75.9	79.19	53	6.5	0.7	67.5	20	55	59.3	61.09
23	11	0.2	120	20	10	65.6	68.01	54	11	0.7	67.5	40	55	86.6	83.17
24	11	1.2	15	20	100	78.4	78.76	55	6.5	0.7	67.5	40	55	63.3	62.06
25	2	0.7	120	20	10	35.7	38.23	56	6.5	0.7	67.5	40	55	62.3	62.06
26	6.5	0.2	67.5	40	55	51.6	51.62	57	6.5	0.7	67.5	40	55	63.9	62.06
27	2	1.2	15	20	10	38.8	36.93	58	6.5	0.7	67.5	60	55	61.5	63.02
28	2	0.2	120	20	100	28.5	28.91	59	6.5	0.7	67.5	40	100	58.6	57.01
29	11	0.2	15	20	10	65.2	67.64	60	6.5	0.7	67.5	40	55	60.8	62.06
30	2	0.2	120	60	10	31.3	31.46	61	6.5	0.7	120	40	55	67.4	62.06
31	2	0.2	15	20	100	27.9	28.54	62	6.5	0.7	67.5	40	55	63.7	62.06

X_1: pH, X_2: TiO2 (gr L^{-1}), X_3: Time (min), X_4: Temperature (℃), X_5: dye concentration (mg L^{-1})

Table 3: Regression analysis for the reduced quadratic model

Model term	Coefficient estimate	Std. error	t-Value	p-Value
Intercept	60.98065	0.42259	144.3030	2.2×10^{-16}
X_1	21.10893	0.37638	56.0848	2.2×10^{-16}
X_2	4.87979	0.38155	12.7895	2.2×10^{-16}
X_3	0.93225	0.37638	2.4769	0.0166787
$X_1:X_2$	1.11835	0.39375	2.8402	0.0065035
$X_2:X_5$	-0.87540	0.39375	-2.2232	0.0307504
$X_3:X_4$	0.75011	0.38809	1.9328	0.0589335
X_2^2	-5.56679	1.13702	-4.8959	1.064×10^{5}
X_3^2	2.23775	1.23870	1.8056	0.0768539
X_5^2	-4.61225	1.23870	-3.7235	0.0004995

Table 4: Analysis of variance (ANOVA) for the reduced quadratic model

Model formula in RSM X_1, X_2, X_3, X_4, X_5	DF	Sum of squares	Mean square	F-value	$F_{critical}$	Probability (P)
First-order response	5	15529.2	3105.84	652.1796	2.40	2.2×10^{-16}
TWI(x1, x2)	1	53.9	53.89	11.3161		0.001482
TWI(x2, x5)	1	15.0	15.00	3.1505		0.081993
TWI(x3, x4)	1	10.1	10.06	2.1130		0.152306
Pure quadratic response	3	940.3	313.54	65.8376		2.2×10^{-16}
Residuals	50	238.1	4.76			
Lack of fit	31	148.7	4.80	1.0196	2.07	0.494661
Pure error	19	89.4	4.71			

Notes: Multiple R-squared: 0.9858, Adjusted R-squared: 0.9827, F-statistic: 315.9on 11 and 50 DF, p-value: $< 2.2\times10^{-16}$

Moreover F-value of the model is significant (F_{cal} = 2150.24 > $F_{0.05, 5, 45}$ = 4.45) and the lack of fit value of the model available in Table 4, is not significant relative to pure error (F_{cal} = 1.09 < $F_{0.05, 26, 19}$ = 2.1) that these are indicated correlation between factors and dye removal as a response (52, 53). In general, the efficiency of the model is explained by R^2, however the multiple R-squared values (0.985) close to one and is very close to the adjusted R-squared value (0.982) anticipated a satisfactory adjustment between quadratic model and experimental data (54, 55). Pareto analysis using the Eq.7 was employed to assess the importance of the role (P_i) of the selected factors (factor i) on the created response.

$$P_i = \left(\frac{\beta_i^2}{\sum \beta_i^2}\right) \qquad (7)$$

As indicated in Fig. 5, the following sequence was gained in the terms containing singular factors X_1 (pH, 77.1%) > X_2 (TiO_2; 12.31%) > X_3 (Time; 0.15%), which approves that pH and TiO_2 plays the most important role among these terms. The quadratic terms have the sequence of X_2^2 (5.35%) > X_5^2 (3.67%) > X_3^2 (0.86%), while the interaction terms have the sequence of X_1X_2 (0.21%) > X_2X_5 (0.13%) > X_3X_4 (0.1%). So the pH, the quadratic TiO_2 and pH-TiO_2 interaction play the most crucial role in the generated response. The results obtained from the Pareto method can be well confirmed by the F-values (56, 57).

3.4 Response Surface Methodology and Contour Plotting

In order to study the effects of different parameters and their interactions on the efficiency of the dye degradation via TiO_2 nanoparticles, the contour plots which are determinate based on the model coefficients is shown in Fig. 6(A-C). It is notable that in these plots the effect of two variables is investigated while the other parameters are stabled (58). The effect of TiO_2 dosage and pH solution on the removal efficiency at the initial time of 67.5 min, temperature of 40 ℃ and dye concentration of 55 mg L^{-1} is shown in Fig 6-A.

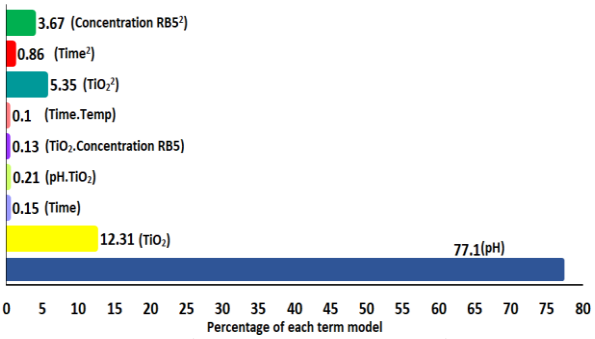

Figure 5: Pareto plot for studying the importance of each variable to the TiO_2 response in the removal of dye

The percentage of dye removal was altered by varying the TiO_2 dosage and pH. As can be understood from the figure in the pH range of 10-11, with an increase of the TiO_2 dosage from 0.8 to 1 gr L^{-1}, removal efficiency was increased from 75 to 80%, in other words, removal efficiency increased with increasing pH. These indications that pH plays an important role in the degradation process (59). Fig. 6(B) illustrations the effects of TiO_2 dosage and dye concentration in the removal efficiency of photo catalyst process. Based on this figure in the TiO_2 dosage of 0.9-1 and at dye concentration of 50-60 mg L^{-1}, removal efficiencies was increased from 62% to 80%. The interaction effects of time (X_3) and temperature (X_4) in Fig. 6(C), illustrations that the percentage of dye removal from 60 to 65% was increased with increasing time from 20 to 120 min. Based on the results, it is clear that the TiO_2 dosage and pH are the most effective variables in the dye removal efficiency (60, 61).

3.5 Process Optimization and Confirmation

The Solver "Add-ins" was used by applying effective parameters to achieve the optimum degraded condition through the model equation predicted by RSM. These parameters contained pH (2-11), TiO_2 dosage (0.2-1.2 g L^{-1}), contact time (15-120 min), temperature (20-60 ℃) and the initial dye concentration (10-100 mg L^{-1}). In the optimum conditions, all parameters simultaneously are favorable criteria, and in the predicted optimal the maximum removal efficiency was accounted to be 90%. The predicted optimal conditions by the Solver "Add-ins" were: the pH of 11, TiO_2 dosage of 0.973 g L^{-1}, contact time of 120 min, temperature 60℃ and initial dye concentration of 50.53 mg L^{-1}. To confirm the validity of the predicted optimum conditions, laboratory experiments were accomplished, and the findings indicated that the experimental data were in good agreement with the above-mentioned optimal conditions (62-64). To verify the validity of the results predicted by the model, additional laboratory experiments were accomplished in four replicates. As it can be understood in Table 5, experimental data were in good consistency with those predicted through the regression model. Furthermore, there is another set of experiments presented in Table 5, which is the same as the above-mentioned optimal conditions except for initial pH.

The result indications that the R-squared value of the model is very near to the adjusted R-squared value. The presence of significant terms in the model was confirmed by the good agreement between R^2adj (0.98) and R^2pred. (0.98) which is presented in Fig. 7 (65).

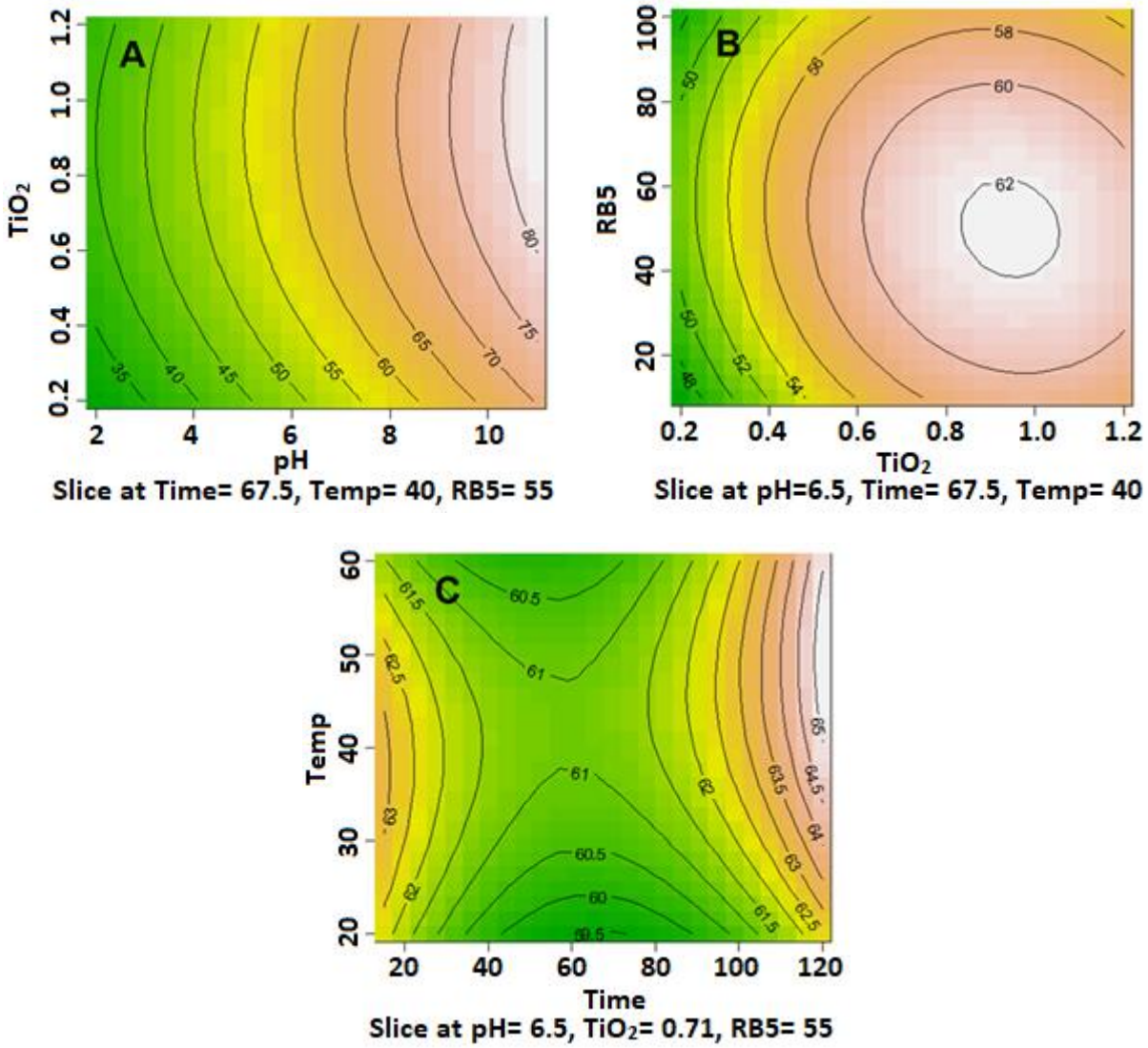

Figure 6: Contour plot for the effect of TiO_2 dose and pH (A), dye concentration and TiO_2 dose (B), time and temperature (C)

Table 5: Experimental and predicted values of the responses at the optimal levels predicted by RSM

					Dye removal (%)	
pH	TiO_2 (g L^{-1})	Time (min)	Temp (℃)	Dye concentration (mg L^{-1})	Predicted	Experimental
11	1	120	60	51	90	87.45
6.5	1	120	60	51	67.93	65.08

4 Conclusions

In this survey, the degradation of dye via TiO_2 nanoparticle at the solid/aqueous interface was studied. The CCD design matrix was accomplished to evaluate the relationship between input-independent factors (pH, TiO_2 dose (g L^{-1}), contact time (min), Temperature (℃), and Dye concentrations (mg L^{-1})) and one dependent output response (removal efficiency) on dye degradation with TiO_2 Photo catalyst. The quadratic equations developed to for this study indicate good correlation between actual and model predicted values of response. The results such as P-value (2.2×10^{-16}), higher F-value (315.9), R^2 (multiple R-squared: 0.9858, adjusted R-squared: 0.9827), insignificant lack of fit (0.494) show that the reduced full second order model is highly significant for dye removal by TiO_2 nanoparticles. The closeness of the R-squared value of the model to the adjusted R-squared value demonstrates that the quadratic regression related to the reduced full second order

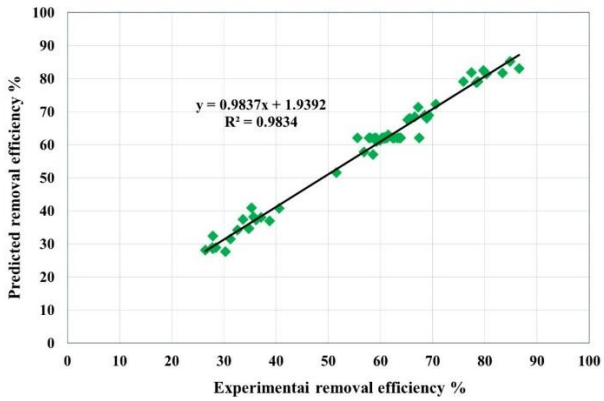

Figure 7: Correlation of actual and predicted removal efficiency for dye direct blue 71

8. Bhatnagar A, Minocha A. Assessment of the biosorption characteristics of lychee (Litchi chinensis) peel waste for the removal of Acid Blue 25 dye from water. Environmental technology. 2010;31(1):97-105.
9. Li W, Li D, Chen Z, Huang H, Sun M, He Y, et al. High-efficient Degradation of Dyes by Zn x Cd1− x S Solid Solutions under Visible Light Irradiation. The Journal of Physical Chemistry C. 2008;112(38):14943-7.
10. Marugán J, López-Muñoz M-J, van Grieken R, Aguado J. Photocatalytic decolorization and mineralization of dyes with nanocrystalline TiO2/SiO2 materials. Industrial & Engineering Chemistry Research. 2007;46(23):7605-10.
11. Devi LG, Kumar SG. Exploring the critical dependence of adsorption of various dyes on the degradation rate using Ln3+-TiO2 surface under UV/solar light. Applied Surface Science. 2012;261:137-46.
12. Jiang Y, Luo Y, Zhang F, Guo L, Ni L. Equilibrium and kinetic studies of CI Basic Blue 41 adsorption onto N, F-codoped flower-like TiO2 microspheres. Applied Surface Science. 2013;273:448-56.
13. Liang C-H, Li F-B, Liu C-S, Lü J-L, Wang X-G. The enhancement of adsorption and photocatalytic activity of rare earth ions doped TiO2 for the degradation of Orange I. Dyes and pigments. 2008;76(2):477-84.
14. Muthirulan P, Devi CN, Sundaram MM. Synchronous role of coupled adsorption and photocatalytic degradation on CAC–TiO2 composite generating excellent mineralization of alizarin cyanine green dye in aqueous solution. Arabian Journal of Chemistry. 2017;10:S1477-S83.
15. Ajoudanian N, Nezamzadeh-Ejhieh A. Enhanced photocatalytic activity of nickel oxide supported on clinoptilolite nanoparticles for the photodegradation of aqueous cephalexin. Materials Science in Semiconductor Processing. 2015;36:162-9.
16. Babaahamdi-Milani M, Nezamzadeh-Ejhieh A. A comprehensive study on photocatalytic activity of supported Ni/Pb sulfide and oxide systems onto natural zeolite nanoparticles. Journal of hazardous materials. 2016;318:291-301.
17. Massoudinejad MR, Sadani M, Gholami Z, Rahmati Z, Javaheri M, Keramati H,et al. Optimization and modeling of photocatalytic degradation of Direct Blue 71 from contaminated water by TiO_2 nanoparticles: Response surface methodology approach (RSM). Iranian Journal of Catalysis. 2019;9(2):121-132.
18. Kordouli E, Bourikas K, Lycourghiotis A, Kordulis C. The mechanism of azo-dyes adsorption on the titanium dioxide surface and their photocatalytic degradation over samples with various anatase/rutile ratios. Catalysis Today. 2015;252:128-35.
19. Belessi V, Romanos G, Boukos N, Lambropoulou D, Trapalis C. Removal of Reactive Red 195 from aqueous solutions by adsorption on the surface of TiO2 nanoparticles. Journal of hazardous materials. 2009;170(2-3):836-44.
20. Carvalho HW, Batista AP, Hammer P, Ramalho TC. Photocatalytic degradation of methylene blue by TiO2–Cu thin films: Theoretical and experimental study. Journal of hazardous materials. 2010;184(1-3):273-80.
21. Othman NH, Alias NH, Shahruddin MZ, Bakar NFA, Him NRN, Lau WJ. Adsorption kinetics of methylene blue dyes onto magnetic graphene oxide. Journal of Environmental Chemical Engineering. 2018;6(2):2803-11.
22. Esmaili-Hafshejani J, Nezamzadeh-Ejhieh A. Increased photocatalytic activity of Zn (II)/Cu (II) oxides and sulfides by coupling and supporting them onto clinoptilolite nanoparticles in the degradation of benzophenone aqueous solution. Journal of hazardous materials. 2016;316:194-203.
23. Zangeneh H, Zinatizadeh A, Habibi M, Akia M, Isa MH. Photocatalytic oxidation of organic dyes and pollutants in wastewater using different modified titanium dioxides: A comparative review. Journal of Industrial and Engineering Chemistry. 2015;26:1-36.
24. Pirkarami A, Olya ME, Farshid SR. UV/Ni–TiO2 nanocatalyst for electrochemical removal of dyes considering operating costs. Water Resources and Industry. 2014;5:9-20.
25. Ba-Abbad MM, Kadhum AAH, Mohamad AB, Takriff MS, Sopian K. Synthesis and catalytic activity of TiO2 nanoparticles for photochemical oxidation of concentrated chlorophenols under direct solar radiation. Int J Electrochem Sci. 2012;7:4871-88.

model can be applied for prediction and optimization. The maximum percentage removal of dye: 86.6% were achieved at optimum operating conditions, pH=11, TiO_2 dose (0.7 g L^{-1}), contact time (67.5 min), Temperature (40 ℃), and dye concentrations (55 mg L^{-1})), respectively. The maximum removal efficiency was predicted to be 90%, using regression coefficients achieved from the model and Solver "Add-ins". The predicted optimal conditions by the Solver "Add-ins" were achieved at the pH of 11, TiO_2 dose of 1 g L^{-1}, contact time of 120 min, Temperature of 60 ℃ and initial dye concentration of 51 mg L^{-1}. So the results indicate that the photocatalytic process is very impressive in eliminating dye from contaminated water, and it has a good efficiency in removing textile dyes.

Acknowledgement

This study is related to the project NO 904003/81 from the Student Research Committee, Ilam University of Medical Sciences, Ilam, Iran. We also appreciate the "Student Research Committee" and "Research & Technology Chancellor" in Ilam University of Medical Sciences for their financial support of this study.

Ethical issue

Authors are aware of, and comply with, best practice in publication ethics specifically with regard to authorship (avoidance of guest authorship), dual submission, manipulation of figures, competing interests and compliance with policies on research ethics. Authors adhere to publication requirements that submitted work is original and has not been published elsewhere in any language.

Competing interests

The authors declare that there is no conflict of interest that would prejudice the impartiality of this scientific work.

Authors' contribution

All authors of this study have a complete contribution for data collection, data analyses and manuscript writing.

References

1. Sharma P, Kaur H, Sharma M, Sahore V. A review on applicability of naturally available adsorbents for the removal of hazardous dyes from aqueous waste. Environmental monitoring and assessment. 2011;183(1-4):151-95.
2. Du Y, Pei M, He Y, Yu F, Guo W, Wang L. Preparation, characterization and application of magnetic Fe3O4-CS for the adsorption of orange I from aqueous solutions. PloS one. 2014;9(12):1160-73.
3. Manikandan G, Kumar S, Saravanan A. Modelling and analysis on the removal of methylene blue dye from aqueous solution using physically/chemically modified Ceiba pentandra seeds. Journal of Industrial and Engineering Chemistry. 2018;62:446-61.
4. Aksu Z, Tatlı Aİ, Tunç Ö. A comparative adsorption/biosorption study of Acid Blue 161: Effect of temperature on equilibrium and kinetic parameters. Chemical Engineering Journal. 2008;142(1):23-39.
5. Guerrero-Coronilla I, Morales-Barrera L, Villegas-Garrido TL, Cristiani-Urbina E. BIOSORPTION OF AMARANTH DYE FROM AQUEOUS SOLUTION BY ROOTS, LEAVES, STEMS AND THE WHOLE PLANT OF E. crassipes. Environmental Engineering & Management Journal (EEMJ). 2014;13(8): 1917-1926.
6. Guerrero-Coronilla I, Morales-Barrera L, Cristiani-Urbina E. Kinetic, isotherm and thermodynamic studies of amaranth dye biosorption from aqueous solution onto water hyacinth leaves. Journal of environmental management. 2015;152:99-108.
7. Srinivasan A, Viraraghavan T. Decolorization of dye wastewaters by biosorbents: a review. Journal of environmental management. 2010;91(10):1915-29.

graphene oxide: equilibrium, kinetic and thermodynamic studies. Journal of colloid and interface science. 2017;496:188-200.
45. Aslani H, Nabizadeh R, Nasseri S, Mesdaghinia A, Alimohammadi M, Mahvi AH, et al. Application of response surface methodology for modeling and optimization of trichloroacetic acid and turbidity removal using potassium ferrate (VI). Desalination and water treatment. 2016;57(52):25317-28.
46. Ghafari S, Aziz HA, Isa MH, Zinatizadeh AA. Application of response surface methodology (RSM) to optimize coagulation–flocculation treatment of leachate using poly-aluminum chloride (PAC) and alum. Journal of hazardous materials. 2009;163(2-3):650-6.
47. Garg KK, Prasad B. Treatment of multicomponent aqueous solution of purified terephthalic acid wastewater by electrocoagulation process: optimization of process and analysis of sludge. Journal of the Taiwan Institute of Chemical Engineers. 2016;60:383-93.
48. Umar M, Aziz HA, Yusoff MS. Assessing the chlorine disinfection of landfill leachate and optimization by response surface methodology (RSM). Desalination. 2011;274(1-3):278-83.
49. Mansoor Ahammed M, Dave S, Nair AT. Effect of water quality parameters on solar water disinfection: a statistical experiment design approach. Desalination and water treatment. 2015;56(2):315-26.
50. Van Thuan T, Quynh BTP, Nguyen TD, Bach LG. Response surface methodology approach for optimization of Cu2+, Ni2+ and Pb2+ adsorption using KOH-activated carbon from banana peel. Surfaces and Interfaces. 2017;6:209-17.
51. Hassani G, Takdastan A, Ghaedi M, Goudarzi G, Neisi A, Babaei AA. Optimization of 4-chlorophenol Oxidation by Manganese Ferrite Nanocatalyst with Response Surface Methodology. Int J Electrochem Sci. 2016;11:8471-85.
52. Senobari S, Nezamzadeh-Ejhieh A. A comprehensive study on the enhanced photocatalytic activity of CuO-NiO nanoparticles: Designing the experiments. Journal of Molecular Liquids. 2018;261:208-17.
53. Nosuhi M, Nezamzadeh-Ejhieh A. An indirect application aspect of zeolite modified electrodes for voltammetric determination of iodate. Journal of Electroanalytical Chemistry. 2018;810:119-28.
54. Senobari S, Nezamzadeh-Ejhieh A. A pn junction NiO-CdS nanoparticles with enhanced photocatalytic activity: A response surface methodology study. Journal of Molecular Liquids. 2018;257:173-83.
55. Nosuhi M, Nezamzadeh-Ejhieh A. Voltammetric determination of trace amounts of permanganate at a zeolite modified carbon paste electrode. New Journal of Chemistry. 2017;41(24):15508-16.
56. Amani-Beni Z, Nezamzadeh-Ejhieh A. Construction of a sensitive non-enzymatic fructose carbon paste electrode–CuO nanoflower: designing the experiments by response surface methodology. New Journal of Chemistry. 2018;42(2):1021-30.
57. Derikvandi H, Nezamzadeh-Ejhieh A. Designing of experiments for evaluating the interactions of influencing factors on the photocatalytic activity of NiS and SnS2: Focus on coupling, supporting and nanoparticles. Journal of colloid and interface science. 2017;490:628-41.
58. Chong SS, Aziz AA, Harun SW, Arof H, Shamshirband S. Application of multiple linear regression, central composite design, and ANFIS models in dye concentration measurement and prediction using plastic optical fiber sensor. Measurement. 2015;74:78-86.
59. Azad FN, Ghaedi M, Dashtian K, Jamshidi A, Hassani G, Montazerozohori M, et al. Preparation and characterization of an AC–Fe 3 O 4–Au hybrid for the simultaneous removal of Cd 2+, Pb 2+, Cr 3+ and Ni 2+ ions from aqueous solution via complexation with 2-((2, 4-dichloro-benzylidene)-amino)-benzenethiol: Taguchi optimization. RSC Advances. 2016;6(24):19780-91.
60. Derikvandi H, Nezamzadeh-Ejhieh A. Comprehensive study on enhanced photocatalytic activity of heterojunction ZnS-NiS/zeolite nanoparticles: experimental design based on response surface methodology (RSM), impedance spectroscopy and GC-MASS studies. Journal of colloid and interface science. 2017;490:652-64.
61. Derikvandi H, Nezamzadeh-Ejhieh A. A comprehensive study on enhancement and optimization of photocatalytic activity of ZnS and SnS2: Response Surface Methodology (RSM), nn
26. Yazdanbakhsh AR, Eslami A, Massoudinejad MR, Avazpour M. Enhanced degradation of sulfamethoxazole antibiotic from aqueous solution using Mn-WO3/LED photocatalytic process: Kinetic, mechanism, degradation pathway and toxicity reduction. Chemical Engineering Journal. 2020;380: 122497.
27. Zabihi-Mobarakeh H, Nezamzadeh-Ejhieh A. Application of supported TiO2 onto Iranian clinoptilolite nanoparticles in the photodegradation of mixture of aniline and 2, 4-dinitroaniline aqueous solution. Journal of Industrial and Engineering Chemistry. 2015;26:315-21.
28. Hosseini SA, Saeedi R. Photocatalytic degradation of rhodamine B by nano bismuth oxide: process modeling by response surface methodology (RSM). Iranian Journal of Catalysis. 2017;7(1):37-46.
29. Nosuhi M, Nezamzadeh-Ejhieh A. High catalytic activity of Fe (II)-clinoptilolite nanoparticales for indirect voltammetric determination of dichromate: Experimental design by response surface methodology (RSM). Electrochimica Acta. 2017;223:47-62.
30. Shan AY, Ghazi TIM, Rashid SA. Immobilisation of titanium dioxide onto supporting materials in heterogeneous photocatalysis: a review. Applied Catalysis A: General. 2010;389(1-2):1-8.
31. Patnaik P. Handbook of environmental analysis: chemical pollutants in air, water, soil, and solid wastes: Crc Press; 2010.
32. Aghabeygi S, KIAKOJORI R, VAKILI AH. SONOSYNTHESIS, CHARACTERIZATION AND PHOTOCATALYTIC DEGRADATION PROPERTY OF NANO ZNO/ZEOLITEA. 2016;6(3):275-279.
33. Rajkumar K, Muthukumar M. Optimization of electro-oxidation process for the treatment of Reactive Orange 107 using response surface methodology. Environmental Science and Pollution Research. 2012;19(1):148-60.
34. Ghafoori S, Mowla A, Jahani R, Mehrvar M, Chan PK. Sonophotolytic degradation of synthetic pharmaceutical wastewater: Statistical experimental design and modeling. Journal of environmental management. 2015;150:128-37.
35. Bandpei AM, Mohseni SM, Sheikhmohammadi A, Sardar M, Sarkhosh M, Almasian M, et al. Optimization of arsenite removal by adsorption onto organically modified montmorillonite clay: Experimental & theoretical approaches. Korean Journal of Chemical Engineering. 2017;34(2):376-83.
36. Moghaddam SS, Moghaddam MA, Arami M. Coagulation/flocculation process for dye removal using sludge from water treatment plant: optimization through response surface methodology. Journal of hazardous materials. 2010;175(1-3):651-7.
37. Nair AT, Makwana AR, Ahammed MM. The use of response surface methodology for modelling and analysis of water and wastewater treatment processes: a review. Water Science and Technology. 2014;69(3):464-78.
38. Zainal-Abideen M, Aris A, Yusof F, Abdul-Majid Z, Selamat A, Omar S. Optimizing the coagulation process in a drinking water treatment plant–comparison between traditional and statistical experimental design jar tests. Water Science and Technology. 2012;65(3):496-503.
39. Abou-Gamra ZM, Ahmed MA. TiO2 nanoparticles for removal of malachite green dye from waste water. Advances in Chemical Engineering and Science. 2015;5(03):373.
40. Park Y, Sun Z, Ayoko GA, Frost RL. Bisphenol A sorption by organo-montmorillonite: implications for the removal of organic contaminants from water. Chemosphere. 2014;107:249-56.
41. Godini H, Hashemi F, Mansuri L, Sardar M, Hassani G, Mohseni S, et al. Water polishing of phenol by walnut green hull as adsorbent: an insight of adsorption isotherm and kinetic. Journal of Water Reuse and Desalination. 2016;6(4):544-52.
42. Petroski J, El-Sayed MA. FTIR study of the adsorption of the capping material to different platinum nanoparticle shapes. The Journal of Physical Chemistry A. 2003;107(40):8371-5.
43. Wang S, Jiang SP, Wang X. Microwave-assisted one-pot synthesis of metal/metal oxide nanoparticles on graphene and their electrochemical applications. Electrochimica Acta. 2011;56(9):3338-44.
44. Konicki W, Aleksandrzak M, Moszyński D, Mijowska E. Adsorption of anionic azo-dyes from aqueous solutions onto

heterojunction, supporting and nanoparticles study. Journal of Photochemistry and Photobiology A: Chemistry. 2017;348:68-78.
62. Wu J, Yu D, Sun H, Zhang Y, Zhang W, Meng F, et al. Optimizing the extraction of anti-tumor alkaloids from the stem of Berberis amurensis by response surface methodology. Industrial Crops and Products. 2015;69:68-75.
63. Naserifar M, Msoudpanah SM, Alamolhoda S. Effect of fuel content on structural and magnetic properties of solution combusted Mn0. 8Zn0. 2Fe2O4 powders. Journal of Ultrafine Grained and Nanostructured Materials. 2018;51(1):26-31.
64. Chen T-S, Tsai R-W, Chen Y-S, Huang K-L. Electrochemical degradation of tetracycline on BDD in aqueous solutions. Int J Electrochem Sci. 2014;9(8422):e8434.
65. Podstawczyk D, Witek-Krowiak A, Dawiec A, Bhatnagar A. Biosorption of copper (II) ions by flax meal: empirical modeling and process optimization by response surface methodology (RSM) and artificial neural network (ANN) simulation. Ecological Engineering. 2015;83:364-79.